Calcif Tissue Int (2011) 89:1–9
DOI 10.1007/s00223-011-9486-0

ORIGINAL RESEARCH

Early Growth Response Gene 1 Regulates Bone Properties in Mice

Marie K. Reumann · Olga Strachna · Lyudmila Lukashova · Kostas Verdelis · Eve Donnelly · Adele L. Boskey · Philipp Mayer-Kuckuk

Received: 17 December 2010 / Accepted: 21 March 2011 / Published online: 2 May 2011

Abstract Transcriptional regulation of the postnatal skeleton is incompletely understood. Here, we determined the consequence of loss of early growth response gene 1 (EGR-1) on bone properties. Analyses were performed on both the microscopic and molecular levels utilizing micro-computed tomography (micro-CT) and Fourier transform infrared imaging (FTIRI), respectively. Mice deficient in EGR-1 (*Egr-1*$^{-/-}$) were studied and compared to sex- and age-matched wild-type (wt) control animals. Femoral trabecular bone in male *Egr-1*$^{-/-}$ mice demonstrated osteopenic characteristics marked by reductions in both bone volume fraction (BV/TV) and bone mineral density (BMD). Morphological analysis revealed fewer trabeculae in these animals. In contrast, female *Egr-1*$^{-/-}$ animals had thinner trabeculae, but BV/TV and BMD were not significantly reduced. Analysis of femoral cortical bone at the mid-diaphysis did not show significant osteopenic characteristics but detected changes in cross-sectional geometry in both male and female *Egr-1*$^{-/-}$ animals. Functionally, this resulted in decreased resistance to three-point bending as indicated by a reduction in maximum load, failure load, and stiffness. Assessment of compositional bone properties, including mineral-to-matrix ratio, carbonate-to-phosphate ratio, crystallinity, and cross-linking, in femurs by FTIRI did not show any significant differences or an appreciable trend between *Egr-1*$^{-/-}$ and wt mice of either sex. Unexpectedly, rib bone from *Egr-1*$^{-/-}$ animals displayed distinct osteopenic traits that were particularly pronounced in female mice. This study provides genetic evidence that both sex and skeletal site are critical determinants of EGR-1 activity in vivo and that its site-specific action may contribute to the mechanical properties of bone.

Keywords Transcription factor · Early growth response gene 1 · Mice · Micro-computed tomography · Biomechanics

Genetic studies in mice have demonstrated that deletion of many immediate early genes such as the AP-1 transcription factor constituents *c-Jun*, *JunB*, and *Fra-1* results in a lethal phenotype [1–3], thereby underscoring their critical role in embryonic development. However, deletion of other immediate early genes, including *c-Fos* and *JunD*, has produced viable mice which presented with, at the time of discovery, unexpected bone abnormalities [4, 5]. Specifically, mice deficient in C-FOS suffer from pronounced osteopetrosis because of a lack of bone-resorbing osteoclasts [5], while animals lacking JUND have high bone mass due to enhanced bone formation [4]. Another immediate early gene potentially involved in postnatal bone biology is *Egr-1*, also known as NGFI-A [6], zif268 [7], krox24 [8], and TIS8 [9]. This transcription factor acts independently of AP-1 and preferentially binds to a GC-rich sequence, 5′-GCGGGGGCG-3′ [10–12], which has been located within the promoter region of a number of

The authors have stated that they have no conflict of interest.

Electronic supplementary material The online version of this article (doi:10.1007/s00223-011-9486-0) contains supplementary material, which is available to authorized users.

M. K. Reumann · O. Strachna · P. Mayer-Kuckuk (✉)
Bone Cell Biology and Imaging Laboratory, Caspary Research Building, Rm. 623, Hospital for Special Surgery, 535 East 70th Street, New York, NY 10021, USA
e-mail: mayerkuckukp@hss.edu

L. Lukashova · K. Verdelis · E. Donnelly · A. L. Boskey
Mineralized Tissue Laboratory, Hospital for Special Surgery, New York, USA

target genes important for proliferation, differentiation, growth control, tumor progression, inflammation, and apoptosis [13–25]. Despite the fact that EGR-1 regulates a broad array of genes in vitro, deficiency of EGR-1 in mice manifests in no visible phenotype and does not alter normal gross appearance, growth rate, and cellular differentiation [21]. However, there is evidence that in stromal cells from these mice a physical interaction between EGR-1 and SP-1 acts as a negative regulator of M-CSF gene expression [26]. Because M-CSF is important for osteoclast formation, this suggests increased osteoclast activity in *Egr-1*$^{-/-}$ mice. Therefore, it is reasonable to hypothesize that EGR-1 functions as a regulator of skeletal properties. Because little is known about the role of EGR-1 in postnatal bone, this study assessed bone structural parameters and composition in both male and female mice. Analyses were carried out on appendicular long bones typically used for mouse phenotype analysis. Additionally, rib, an axial flat bone, was assessed to derive data from a distant skeletal site.

Materials and Methods

Animal Model

Heterozygous breeding pairs of the *Egr-1*$^{-/-}$ mouse model 2013 (B6 background) were originally purchased from Taconic (Hudson, NY). Wild-type (wt, +/+) and *Egr-1*$^{-/-}$ mice were derived from an in-house colony through a het/het breeding scheme and identified by standard genotyping procedures using polymerase chain reaction. Animal work was performed in accordance with the Institutional Animal Care and Use Committee. All animals for this study were offspring of the established mouse colony. Having reached the age of 12–14 weeks and prior to death, the body weight of animals was measured using a digital scale.

Tissue Preparation

All mice were killed using CO_2 inhalation. Femurs were harvested by disarticulation of the femur in the hip joint to separate the lower limb from the torso. The patella tendon was cut horizontally and the tibia was separated from the femur. Subsequently, all surrounding muscle was removed. For rib tissue preparation a longitudinal incision was made along the thoracic spine, thereby exposing the dorsal aspect of the thorax. Ribs were counted from caudal to cranial to identify an eighth rib. For harvesting, tissue was dissected with scissors. Subsequently, all surrounding skeletal muscle was removed. For initial bone-length measurements, a manual caliper was utilized.

Radiography and Micro-Computed Tomography

A total of six male and seven female *Egr-1*$^{-/-}$ bones were studied per group. The same numbers of age- and sex-matched wt bones from littermates served as controls. For radiography and subsequent micro-computed tomography (micro-CT), tibia, femur, and eighth rib were used. Radiography was performed with the MX20 Faxitron (Lincolnshire, IL) system at 26 kVp and 10 s with automatic exposure control. All bones were stored in 70% ethanol at 4°C until subjected to micro-CT analysis. Three-dimensional (3D) morphology of trabecular and cortical bones was determined within a 1.2-mm region of interest (ROI) defined at the distal epiphysis of the femurs starting 100 μm from the growth plate, a 1-mm ROI at the mid-diaphysis, and 3 mm of the middle section of the eighth rib using a Scanco μCT 35 (Scanco Medical, Bassersdorf, Switzerland) desktop system. All bones were scanned in 70% ethanol. A 6-μm voxel size, 55 kVp, 0.36° rotation step, 180° angular range, 400-ms exposure, and three averaged frames per view were used. The Scanco μCT software was used for 3D reconstruction, evaluation, and viewing of images. After 3D reconstruction, volumes of interest were segmented and analyzed using a global threshold of 0.4 g cm^{-3} for trabecular bone and 0.6 g cm^{-3} for cortical bone. In addition to bone mineral density (BMD, mg ml^{-1}), bone morphometric measurements, including bone volume fraction (BV/TV, %), surface to volume ratio (BS/BV, mm^{-1}), trabecular thickness (Tb.Th, mm), trabecular number (Tb.N, mm^{-1}), trabecular separation (Tb.Sp, mm), and connectivity density (Conn.D, mm^{-3}), were calculated for trabecular bone. For cortical and rib bone assessment, BMD, BV/TV [27], cortical thickness (Th, mm), maximum (I_{max}, mm^4) and minimum (I_{min}, mm^4) moments of inertia, and bone area (BA, mm^2) were measured.

Fourier Transform Infrared Spectroscopic Imaging

Three male and three female animals form each genotype (−/− and wt) were randomly selected from the same animal cohort that was used for micro-CT, and the contralateral femur was prepared for FTIRI. All specimens were fixed with an alcohol gradient and embedded in polymethyl methacrylate. Embedded specimens were cut into 2-μm-thick sections using a microtome (SM2500; Leica, Bannockburn, IL) and mounted on barium fluoride infrared windows (SpectraTech, Hopewell Junction, NY). Sections were analyzed by FTIRI using a Spotlight 300 Imaging system (Perkin-Elmer Instruments, Waltham, MA). Based on a light microscopic micrograph of each section, femoral trabecular and cortical ROIs approximately corresponding to the micro-CT ROIs were scanned from 2000 to 800 cm^{-1} at a spectral resolution of 4 cm^{-1} and a spatial

resolution of 6.25 μm as described elsewhere [28]. Because of possible variation in section thickness, we measured only relative spectroscopic parameters that were characterized before [29]. Briefly, those parameters included the mineral-to-matrix ratio, crystallinity, carbonate-to-phosphate ratio, and (collagen) cross-linking, which correlate with relative bone mineral content, mineral crystal size and perfection, carbonate substitution in hydroxyapatite, and collagen maturity, respectively [30]. After spectral subtraction of the embedding medium followed by spatial and spectral masking of the background in every scanned field, the spectroscopic results were expressed as mean values and standard deviations of the pixel distributions; and corresponding color-coded images were generated using ISYS software (Olney, MD). In addition, heterogeneity of FTIRI parameters was assessed by the full width at half-maximum calculated from the pixel histograms for each individual image [31]. Means and standard deviations were averaged for multiple sites in each animal for areas of cortical and trabecular bone.

Mechanical Testing

Mechanical properties of femurs were evaluated by three-point bending tests for wt ($n = 6$) and *Egr-1*$^{-/-}$ ($n = 6$) bones. Tests were conducted at room temperature on a precision electromagnet-based load frame (EnduraTEC ELF 3200; Bose, Minnetonka, MN). Femurs were tested such that the anterior side was loaded in compression and the posterior side in tension. The posterior surface was placed on the lower supports, which were set 7.61 mm apart for both wt and *Egr-1*$^{-/-}$ bones. Load was applied at 0.1 mm s^{-1} until failure occurred, and data were recorded at 100 data points/s. Structural mechanical properties that are dependent on geometry were measured and included max load (N), failure load (N), stiffness (N mm^{-1}), max moment (N mm), and failure moment (N mm).

Statistical Analysis

Statistical analyses were carried out using a two-sample *t*-test, assuming equal variance; $P < 0.05$ was considered significant.

Results

Mice Deficient in EGR-1 Present with a Reduction in Body Weight

Male *Egr-1*$^{-/-}$ mice measured a 13.5% reduction in body weight compared to wt male animals (Fig. 1a). A 13.7% weight reduction was also recorded for female *Egr-1*$^{-/-}$ mice (Fig. 1a). Comparing the two sexes, female *Egr-1*$^{-/-}$ mice were 11.5% lighter than male *Egr-1*$^{-/-}$ mice, an expected finding that reflects the natural weight difference between female and male wt mice (Fig. 1a). Post mortem radiographic analysis was used for initial phenotype screening. No obvious differences were detected between knockout and wt femurs or ribs of either sex (Fig. 1b). A similar observation was made for tibias (data not shown). Assessment of bone length also did not reveal any significant difference between knockout and wt femurs or ribs in either male or female mice (Fig. 1c).

Reduced BV and BMD in Trabecular Bone of *Egr-1*$^{-/-}$ Male Mice

To determine the consequence of EGR-1 deficiency on the mouse skeleton, we first performed bone measurements using micro-CT. A significantly (43%) reduced BV/TV was detected in femoral trabecular bone in male *Egr-1*$^{-/-}$ mice compared to male wt animals (Fig. 2a). This was also the case for tibial trabecular bone (data not shown). Along with the decrease in BV/TV, a statistically significant 4% lower BMD was observed in trabecular, but not cortical, bone of male *Egr-1*$^{-/-}$ mice (Fig. 2c, d). In contrast to male mice, no significant reduction in BV/TV or BMD was measured for trabecular or cortical bone in female mice (Fig. 2a–d). Planes roughly located within the ROI examined by micro-CT were analyzed on the molecular level utilizing FTIRI to detect changes in mineral-to-matrix ratio, carbonate-to-phosphate ratio, crystallinity, or cross-linking. There was no statistically significant change in any of these parameters between *Egr-1*$^{-/-}$ and wt femur trabecular (Table 1) or cortical (Table 2) bone. For each parameter, we then compared the signal distribution (heterogeneity) within each ROI by visually inspecting the corresponding images and found a modest reduction in heterogeneity of the mineral-to-matrix ratio in *Egr-1*$^{-/-}$ compared to wt cortical bone of the female femur (Supplementary Fig. 1). This prompted us to quantify signal heterogeneity for all parameters (not shown). A statistically significant decrease in heterogeneity of 16% ($P = 0.04$) was only observed for the mineral-to-matrix ratio in female *Egr-1*$^{-/-}$ femur cortical bone.

Sex-Specific Alterations Cause Low Trabecular BV in *Egr-1*$^{-/-}$ Mice

To investigate the origin of the reduction of BV/TV in trabecular bone, a more detailed micro-CT analysis of the trabecular morphology was conducted (Fig. 3). Trabeculae from male *Egr-1*$^{-/-}$ mice showed a significant 17% reduction in number (Fig. 3a), associated with a 23% larger separation (Fig. 3c). As a result, the density of trabecular connections was also reduced (Fig. 3e). Additionally,

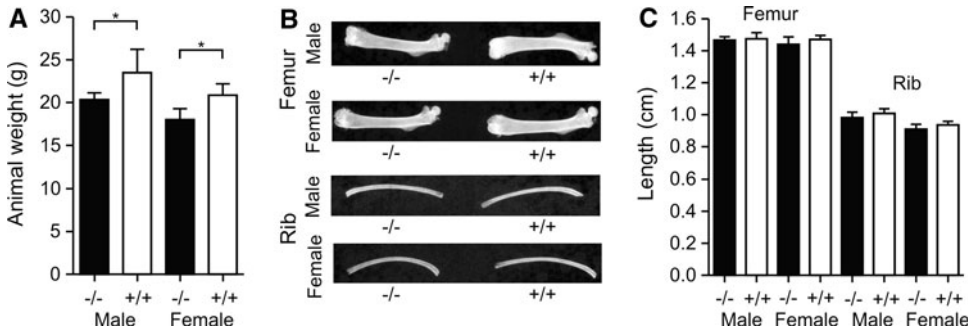

Fig. 1 Weight reduction and normal bony gross appearance in *Egr-1*$^{-/-}$ compared to wt (+/+) mice. **a** Animal weight at death. **b** Bone anatomy captured by radiography. **c** Overall length of excised bones was evaluated in male and age-matched female animals

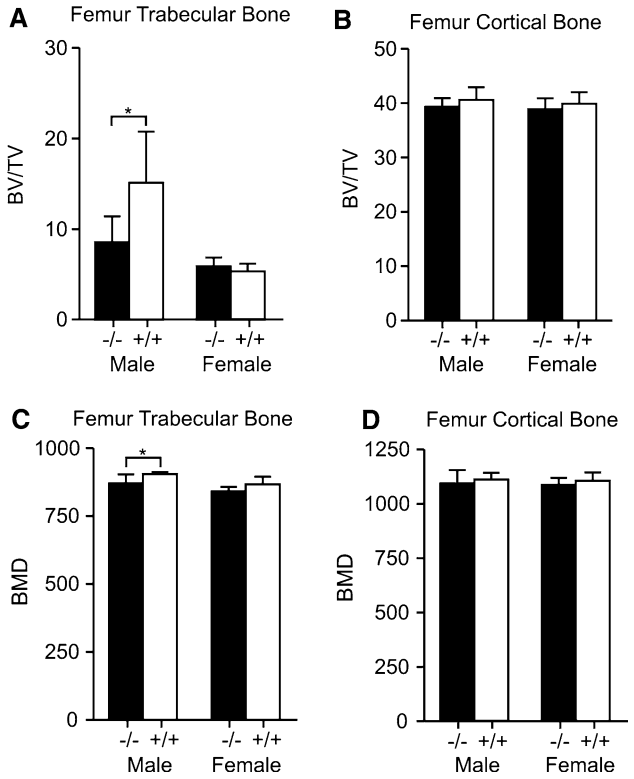

Fig. 2 Osteopenic bone characteristics in male *Egr-1*$^{-/-}$ mice. Micro-CT measurements are presented and expressed as mean ± standard deviation. Statistical comparisons were made for each knockout (−/−) and wild-type (+/+) comparison, but only statistically significant (*$P < 0.05$) differences are indicated

thinner trabeculae were noted, but this observation was not significant (Fig. 3b). Trabecular bone from female *Egr-1*$^{-/-}$ femurs was chiefly characterized by an 11% loss in thickness (Fig. 3b), which correlated to a 7% increase in BS/BV ratio (Fig. 3d). Although statistically not significant, there was a tendency for compensation as indicated by an increase in trabecular number (Fig. 3a) and a decrease in separation (Fig. 3c).

Functional Abnormalities in the Cross-Sectional Geometry of Cortical *Egr-1*$^{-/-}$ Bone

To assess the basis of the reduction of BV/TV in femur cortical bone, an extended micro-CT analysis of the cortical bone geometry was carried out (Fig. 4a–d). Statistically significant reductions of 10, 29, and 17% were seen for bone area in females and the minimum moment of inertia in males and females, respectively. Because the observed changes in cross-sectional geometry can influence the biomechanical properties of bone, three-point bending to failure was conducted on male *Egr-1*$^{-/-}$ femurs, which showed the most pronounced reduction in the minimum moment of inertia. Testing revealed statistically significant reductions of 28, 42, 33, 28, and 42% in maximum load, failure load, stiffness, maximum moment, and failure moment, respectively (Fig. 4e–i). Hence, in male femurs, the loss of EGR-1 produced a change in cross-sectional geometry that led to reduced bending stiffness and strength during three-point bending.

Alterations in Female Rib Cortical Bone Differ from Femur Cortical Bone

In rib bone, micro-CT revealed 8 and 14% reductions in BV/TV in male and female *Egr-1*$^{-/-}$ animals, respectively

Table 1 FTIR parameters ± standard deviation for trabecular bone

	Male			Female		
	Egr-1$^{-/-}$ (mean ± SD)	Wild type (mean ± SD)	*P*	*Egr-1*$^{-/-}$ (mean ± SD)	Wild type (mean ± SD)	*P*
Mineral-to-matrix	4.862 ± 0.2944	4.609 ± 0.2275	0.30	4.470 ± 0.1138	4.498 ± 0.6343	0.94
Carbonate-to-phosphate	0.005861 ± 0.000189	0.005876 ± 0.000098	0.91	0.005780 ± 0.0009994	0.005562 ± 0.0003477	0.74
Crystallinity	1.159 ± 0.00957	1.135 ± 0.02088	0.14	1.113 ± 0.04613	1.145 ± 0.03039	0.37
Cross-linking	4.176 ± 0.07934	4.489 ± 0.2841	0.14	4.377 ± 0.1713	4.776 ± 0.3797	0.17

Table 2 FTIR parameter ± standard deviation for cortical bone

	Male			Female		
	Egr-1$^{-/-}$ (mean ± SD)	Wild type (mean ± SD)	*P*	*Egr-1*$^{-/-}$ (mean ± SD)	Wild type (mean ± SD)	*P*
Mineral-to-matrix	6.342 ± 0.3952	6.195 ± 0.03748	0.56	6.560 ± 0.1599	6.556 ± 0.3736	0.99
Carbonate-to-phosphate	0.006641 ± 0.0003483	0.006824 ± 0.0002305	0.49	0.007041 ± 0.0005063	0.006824 ± 0.0001264	0.51
Crystallinity	1.186 ± 0.02	1.189 ± 0.01718	0.84	1.151 ± 0.02987	1.172 ± 0.007234	0.30
Cross-linking	3.933 ± 0.1904	4.057 ± 0.186	0.47	3.912 ± 0.09563	4.072 ± 0.1329	0.17

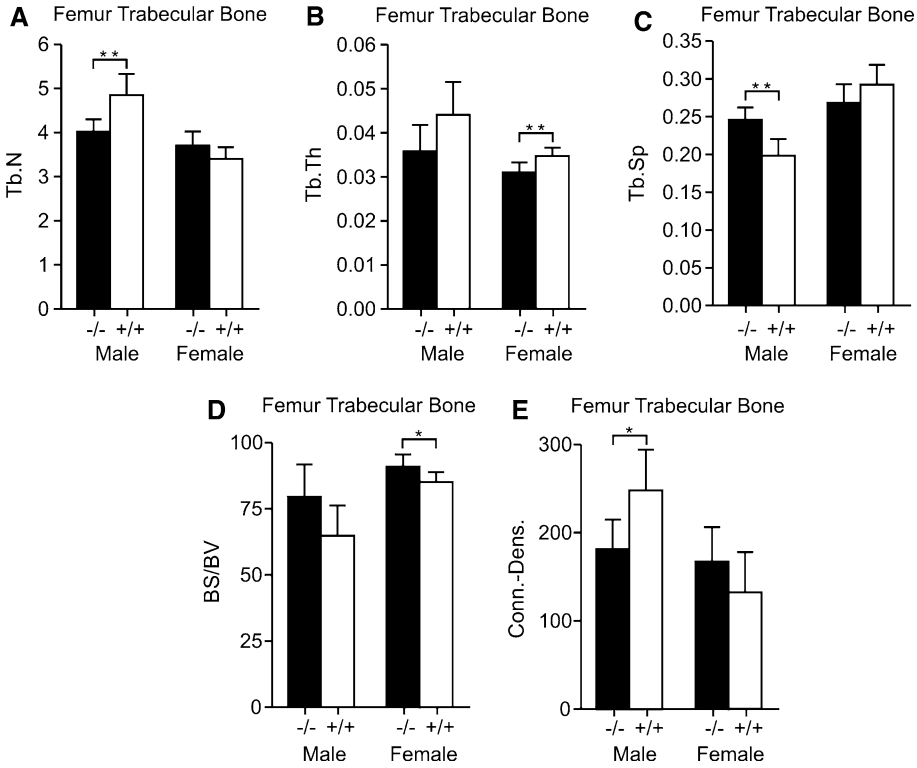

Fig. 3 Trabecular bone morphology in EGR-1-deficient bones is sex-dependent. Micro-CT measurements are presented and expressed as mean ± standard deviation. Statistical comparisons were made for each knockout (−/−) and wild-type (+/+) comparison, but only statistically significant (*$P < 0.05$, **$P < 0.001$) differences are indicated

(Fig. 5a), compared to no significant change in femur cortical bone (Fig. 2b). Similar to femurs, however, no alteration in BMD was observed in either male or female ribs (Fig. 5b). With an 8% decrease in males compared to 17% in females, thickness was less affected in male ribs (Fig. 5c). A 20% reduction in bone area was seen in female, but not in male, *Egr-1*$^{-/-}$ mice (Fig. 5d). Cross-sectional geometry in male *Egr-1*$^{-/-}$ mice was not altered compared to wt mice (Fig. 5e, f), while female *Egr-1*$^{-/-}$ animals had a 21% decreased minimum moment of inertia (Fig. 5f). Thus, compared to femur cortical bone, rib cortical bone showed decreased bone mass and, in female animals, distinct geometrical changes.

Discussion

In this study, we used a genetic approach to investigate the hypothesis that EGR-1 functions as a regulator of the postnatal skeleton. Bone properties were compared between wt and *Egr-1*$^{-/-}$ mice at approximately 3 months of age. This time point was chosen because it permitted comparison to relevant published data [32]. Further, a single–time point examination freed resources for in-depth measurements at multiple skeletal sites in both male and female animals. Mice deficient in EGR-1 were smaller than wt mice, but femurs, tibias, and ribs presented with a normal gross appearance (Fig. 1b, c, and unpublished data). Across these three bone types, a net osteopenic phenotype was observed, as characterized by a reduction in BV/TV in all male and female bones except female trabecular bone (Figs. 2a, b and 5a; see supplementary tables). Further, BMD was reduced in all male and female bones except male rib bones (Figs. 2c, d and 5b; see supplementary tables). This observation is consistent with a previous report by Cenci et al. [32], who measured BMD over the hind limb of *Egr-1*$^{-/-}$ and wt mice of comparable age and found a reduction in *Egr-1*$^{-/-}$ animals. They also described an increase in both

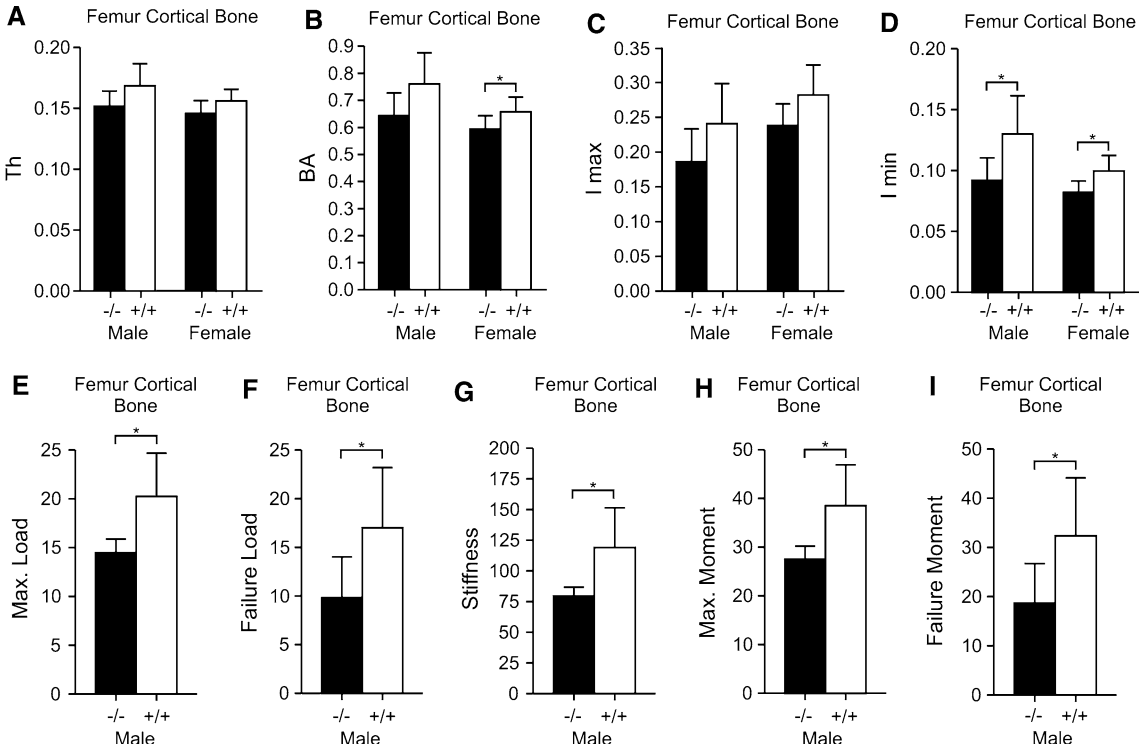

Fig. 4 Abnormalities in the cross-sectional geometry of cortical *Egr-1*$^{-/-}$ bone. **a–d** Micro-CT measurements are presented and expressed as mean ± standard deviation. **e–i** Mechanical properties of the male femur as determined by three-point bending. Statistical comparisons were made for each knockout (−/−) and wild-type (+/+) comparison, but only statistically significant (*$P < 0.05$, **$P < 0.001$) differences are indicated

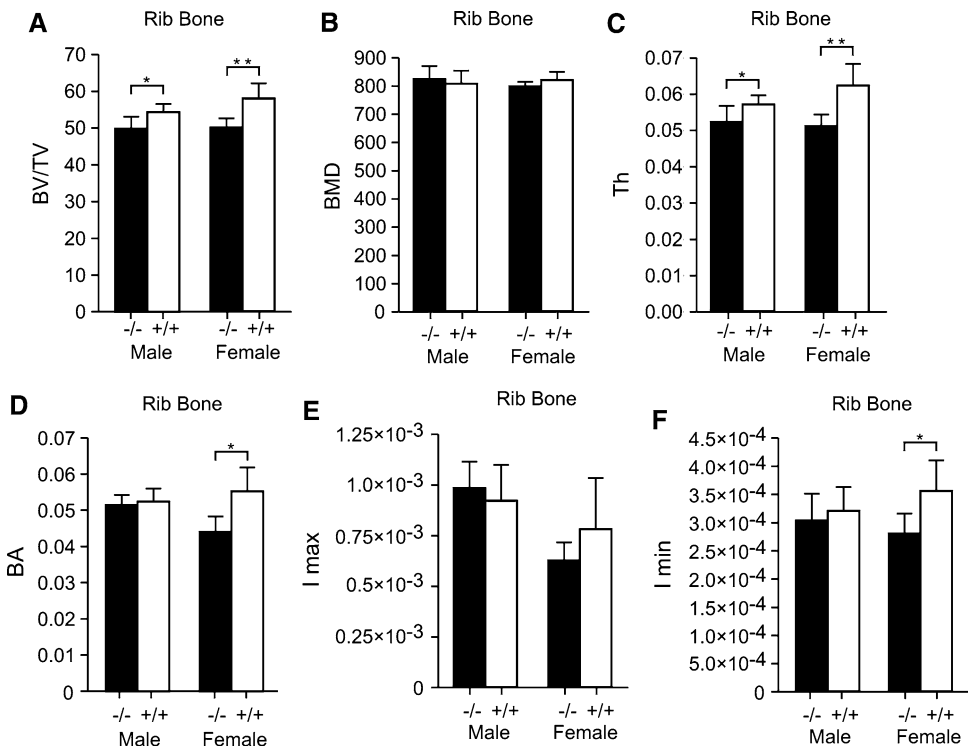

Fig. 5 Distinct osteopenic traits in rib bone. Micro-CT measurements are presented and expressed as mean ± standard deviation. Statistical comparisons were made for each knockout (−/−) and wild-type (+/+) comparison, but only statistically significant (*$P < 0.05$, **$P < 0.001$) differences are indicated

excretion of deoxypyridinoline and serum levels of osteocalcin in *Egr-1*$^{-/-}$ mice [32], potentially suggestive of a bone turnover defect. However, there is no stringent correlation between detection of circulating bone turnover markers and a bone phenotype [33], perhaps, at least in part, because of a temporal or spatial divergence. Thus, in future studies it will be important to accurately compare *Egr-1*$^{-/-}$ and wt mice for bone-turnover abnormalities using dynamic histomorphometry. Although we did not directly measure cellular markers of bone turnover, the use of FTIRI [29] permitted assessment of bone properties at the molecular level. This has been shown to be a sensitive method [34] for detection of bone-turnover abnormalities in rodent [35, 36] and human [37] bones. Our data did not reveal any difference in mineral-to-matrix ratio, carbonate-to-phosphate ratio, crystallinity, or cross-linking, which is a measure of collagen maturity (Table 1). Neither did the data suggest a trend toward a significant alteration in one of these molecular parameters. However, the analysis was based on a sample size of three, which is a limitation of the study. Hence, we cannot exclude the possibility that larger sample sizes may reveal differences in one of the molecular parameters. Together, loss of EGR-1 resulted in osteopenia without significantly affecting the molecular properties of bone. Such phenotypes have been reported before. For example, overexpression of the vitamin D receptor in mature osteoblasts resulted in increased BV/TV in mice [33], without affecting FTIRI parameters in cortical bone and a sole decrease in collagen maturity in trabecular bone [38], although changes in mineral crystal structure were detected by X-ray diffraction. Similar to EGR-1, vitamin D receptor is a convergence point between cellular signaling and gene-expression programs [39, 40].

A sex-specific function of EGR-1 was observed in trabecular bone of the femur. Male, but not female, *Egr-1*$^{-/-}$ mice showed an osteopenic phenotype characterized by a statistically significant decrease in both BV/TV and BMD. Why female EGR-1-deficient mice are protected from bone loss is unclear. However, the study by Cenci et al. [32] showed that ovariectomy of *Egr-1*$^{-/-}$ mice did not result in bone loss, suggesting that a minimal bone mass is guarded from further decrease. This may relate to our observations because a significant reduction of trabecular BV/TV was observed in wt female mice compared to wt male animals (Fig. 2a) and it is possible that the reduced female bone mass is shielded from further EGR-1-related reduction. In comparison to femur trabecular bone, femur cortical bone and rib bone BV/TV did not differ between wt male and female mice. Consistent with this observation, osteopenic characteristics were seen in both male and female rib bones of *Egr-1*$^{-/-}$ mice (Fig. 5a). They were, however, statistically more distinct in female compared to male animals (Fig. 5a), a finding that needs further investigation.

Male and female bone properties were initially studied by micro-CT in femur (Figs. 2, 3, and 4) and tibia (see supplementary tables), both appendicular long bones. Measurements on femurs and tibias yielded very similar results. For example, in cortical bone the direction of change as well as the significance of all assessed parameters were identical between femur (Figs. 2, 4) and tibia (Supplementary Table 1). In contrast, rib bones showed a distinct alteration signature between *Egr-1*$^{-/-}$ and wt mice (Fig. 5), suggesting a site-specific influence of EGR-1. Our study included ribs because they have been the subject of previous investigations, such as pharmacological studies of bisphosphonates [41, 42] and bone fracture healing [43, 44]. Very little, however, is known about rib bone biology, which makes it challenging to interpret our data regarding potential site-specific differences in bone biology that may explain the differential magnitude or specificity of EGR-1 activity between appendicular long bones and rib. Nevertheless, site-specific differences in bone cell activity have been reported before and are particularly well established for osteoclasts, although the mechanisms underlying these differences are largely unknown but may include variation in developmental origin, precursor populations, mechanical load, or hormonal activity [45]. Interestingly, early work by Wiktor-Jedrzejczak et al. suggested that the efficacy of rescue of the osteopetrotic phenotype of op/op mice with M-CSF was site-specific [46, 47]. Assuming loss of EGR-1 provokes a site-specific increase in M-CSF production [26], our findings are in line with these data. More recent work, however, indicates that site-specific differences in bone cell activity may stem from development-based gene-expression signatures, which are distinct for particular bones [48]. Further, studying human bones, Varanasi et al. [49] showed that site-specific alterations were due to differences in multiple signaling pathways rather than just cell numbers. Notably, a computational assessment of these signaling pathways using network-generating algorithms suggested, consistent with the present report, an involvement of EGR-1 in bone cell biology [49]. An important question is whether EGR-1 plays a functional role in the skeleton. We noted a significant reduction in the minimum moment of inertia in male cortical bone of the femur (Fig. 4d), which was suggestive of an alteration in mechanical properties. Subsequent testing revealed a decrease in several mechanical testing parameters during three-point bending (Fig. 4e–i). Hence, it is likely that the changes in cross-sectional geometry are the cause for the reduced resistance to three-point bending, but we also detected a small change in bone heterogeneity; thus, we cannot rule out the possibility that other factors may contribute to the observed change in femur mechanical properties. All together, this study demonstrated that both sex and skeletal site determine EGR-1 activity in vivo

and that its site-specific action may influence the mechanical properties of bone.

Acknowledgements We thank Kirsten Stoner for skilled execution and interpretation of mechanical bone testing, Ashley Acosta for expert data collection and analysis, and Dr. Marjolein van der Meulen for critical comments on the manuscript. This work was supported by NIH grants R01AR055294 (P. M.-K.) and P30AR046121 (A. L. B.) as well as the postdoctoral fellowship F32AR056148 (E. D.).

References

1. Wagner EF (2010) Bone development and inflammatory disease is regulated by AP-1 (Fos/Jun). Ann Rheum Dis 69(Suppl 1):i86–i88
2. Wagner EF (2002) Functions of AP1 (Fos/Jun) in bone development. Ann Rheum Dis 61(Suppl 2):ii40–ii42
3. Karsenty G (2008) Transcriptional control of skeletogenesis. Annu Rev Genomics Hum Genet 9:183–196
4. Kawamata A, Izu Y, Yokoyama H, Amagasa T, Wagner EF, Nakashima K, Ezura Y, Hayata T, Noda M (2008) JunD suppresses bone formation and contributes to low bone mass induced by estrogen depletion. J Cell Biochem 103:1037–1045
5. Wang ZQ, Ovitt C, Grigoriadis AE, Mohle-Steinlein U, Ruther U, Wagner EF (1992) Bone and haematopoietic defects in mice lacking c-fos. Nature 360:741–745
6. Milbrandt J (1987) A nerve growth factor-induced gene encodes a possible transcriptional regulatory factor. Science 238:797–799
7. Lau LF, Nathans D (1987) Expression of a set of growth-related immediate early genes in BALB/c 3T3 cells: coordinate regulation with c-fos or c-myc. Proc Natl Acad Sci USA 84:1182–1186
8. Lemaire P, Revelant O, Bravo R, Charnay P (1988) Two mouse genes encoding potential transcription factors with identical DNA-binding domains are activated by growth factors in cultured cells. Proc Natl Acad Sci USA 85:4691–4695
9. Lim RW, Varnum BC, Herschman HR (1987) Cloning of tetradecanoyl phorbol ester-induced "primary response" sequences and their expression in density-arrested Swiss 3T3 cells and a TPA non-proliferative variant. Oncogene 1:263–270
10. Christy B, Nathans D (1989) DNA binding site of the growth factor-inducible protein Zif268. Proc Natl Acad Sci USA 86:8737–8741
11. Gashler A, Sukhatme VP (1995) Early growth response protein 1 (Egr-1): prototype of a zinc-finger family of transcription factors. Prog Nucleic Acid Res Mol Biol 50:191–224
12. Swirnoff AH, Milbrandt J (1995) DNA-binding specificity of NGFI-A and related zinc finger transcription factors. Mol Cell Biol 15:2275–2287
13. Gururajan M, Simmons A, Dasu T, Spear BT, Calulot C, Robertson DA, Wiest DL, Monroe JG, Bondada S (2008) Early growth response genes regulate B cell development, proliferation, and immune response. J Immunol 181:4590–4602
14. Hofer G, Grimmer C, Sukhatme VP, Sterzel RB, Rupprecht HD (1996) Transcription factor Egr-1 regulates glomerular mesangial cell proliferation. J Biol Chem 271:28306–28310
15. Ham J, Eilers A, Whitfield J, Neame SJ, Shah B (2000) c-Jun and the transcriptional control of neuronal apoptosis. Biochem Pharmacol 60:1015–1021
16. Scharnhorst V, Menke AL, Attema J, Haneveld JK, Riteco N, van Steenbrugge GJ, van der Eb AJ, Jochemsen AG (2000) EGR-1 enhances tumor growth and modulates the effect of the Wilms' tumor 1 gene products on tumorigenicity. Oncogene 19:791–800
17. Biesiada E, Razandi M, Levin ER (1996) Egr-1 activates basic fibroblast growth factor transcription. Mechanistic implications for astrocyte proliferation. J Biol Chem 271:18576–18581
18. Perez-Castillo A, Pipaon C, Garcia I, Alemany S (1993) NGFI-A gene expression is necessary for T lymphocyte proliferation. J Biol Chem 268:19445–19450
19. Kaufmann K, Thiel G (2001) Epidermal growth factor and platelet-derived growth factor induce expression of Egr-1, a zinc finger transcription factor, in human malignant glioma cells. J Neurol Sci 189:83–91
20. Kaufmann K, Thiel G (2002) Epidermal growth factor and thrombin induced proliferation of immortalized human keratinocytes is coupled to the synthesis of Egr-1, a zinc finger transcriptional regulator. J Cell Biochem 85:381–391
21. Lee SL, Tourtellotte LC, Wesselschmidt RL, Milbrandt J (1995) Growth and differentiation proceeds normally in cells deficient in the immediate early gene NGFI-A. J Biol Chem 270:9971–9977
22. Cibelli G, Policastro V, Rossler OG, Thiel G (2002) Nitric oxide-induced programmed cell death in human neuroblastoma cells is accompanied by the synthesis of Egr-1, a zinc finger transcription factor. J Neurosci Res 67:450–460
23. Messmer UK, Brune B (1996) Nitric oxide-induced apoptosis: p53-dependent and p53-independent signalling pathways. Biochem J 319(Pt 1):299–305
24. Le-Niculescu H, Bonfoco E, Kasuya Y, Claret FX, Green DR, Karin M (1999) Withdrawal of survival factors results in activation of the JNK pathway in neuronal cells leading to Fas ligand induction and cell death. Mol Cell Biol 19:751–763
25. Behrens A, Sibilia M, Wagner EF (1999) Amino-terminal phosphorylation of c-Jun regulates stress-induced apoptosis and cellular proliferation. Nat Genet 21:326–329
26. Srivastava S, Weitzmann MN, Kimble RB, Rizzo M, Zahner M, Milbrandt J, Ross FP, Pacifici R (1998) Estrogen blocks M-CSF gene expression and osteoclast formation by regulating phosphorylation of Egr-1 and its interaction with Sp-1. J Clin Invest 102:1850–1859
27. Hoenderop JG, van Leeuwen JP, van der Eerden BC, Kersten FF, van der Kemp AW, Merillat AM, Waarsing JH, Rossier BC, Vallon V, Hummler E, Bindels RJ (2003) Renal Ca^{2+} wasting, hyperabsorption, and reduced bone thickness in mice lacking TRPV5. J Clin Invest 112:1906–1914
28. Gourion-Arsiquaud S, West PA, Boskey AL (2008) Fourier transform-infrared microspectroscopy and microscopic imaging. Methods Mol Biol 455:293–303
29. Boskey A, Pleshko Camacho N (2007) FT-IR imaging of native and tissue-engineered bone and cartilage. Biomaterials 28:2465–2478
30. Boskey A, Mendelsohn R (2005) Infrared analysis of bone in health and disease. J Biomed Opt 10:031102
31. Gourion-Arsiquaud S, Allen MR, Burr DB, Vashishth D, Tang SY, Boskey AL (2010) Bisphosphonate treatment modifies canine bone mineral and matrix properties and their heterogeneity. Bone 46:666–672
32. Cenci S, Weitzmann MN, Gentile MA, Aisa MC, Pacifici R (2000) M-CSF neutralization and egr-1 deficiency prevent ovariectomy-induced bone loss. J Clin Invest 105:1279–1287
33. Gardiner EM, Baldock PA, Thomas GP, Sims NA, Henderson NK, Hollis B, White CP, Sunn KL, Morrison NA, Walsh WR, Eisman JA (2000) Increased formation and decreased resorption of bone in mice with elevated vitamin D receptor in mature cells of the osteoblastic lineage. FASEB J 14:1908–1916
34. Boskey AL, Spevak L, Paschalis E, Doty SB, McKee MD (2002) Osteopontin deficiency increases mineral content and mineral crystallinity in mouse bone. Calcif Tissue Int 71:145–154
35. Anderson HC, Sipe JB, Hessle L, Dhanyamraju R, Atti E, Camacho NP, Millan JL (2004) Impaired calcification around

matrix vesicles of growth plate and bone in alkaline phosphatase-deficient mice. Am J Pathol 164:841–847
36. Camacho NP, Rimnac CM, Meyer RA Jr, Doty S, Boskey AL (1995) Effect of abnormal mineralization on the mechanical behavior of X-linked hypophosphatemic mice femora. Bone 17:271–278
37. Boskey AL, DiCarlo E, Paschalis E, West P, Mendelsohn R (2005) Comparison of mineral quality and quantity in iliac crest biopsies from high- and low-turnover osteoporosis: an FT-IR microspectroscopic investigation. Osteoporos Int 16:2031–2038
38. Misof BM, Roschger P, Tesch W, Baldock PA, Valenta A, Messmer P, Eisman JA, Boskey AL, Gardiner EM, Fratzl P, Klaushofer K (2003) Targeted overexpression of vitamin D receptor in osteoblasts increases calcium concentration without affecting structural properties of bone mineral crystals. Calcif Tissue Int 73:251–257
39. Lian JB, Stein GS (1992) Transcriptional control of vitamin D-regulated proteins. J Cell Biochem 49:37–45
40. Khachigian LM, Collins T (1998) Early growth response factor 1: a pleiotropic mediator of inducible gene expression. J Mol Med 76:613–616
41. Mashiba T, Hirano T, Turner CH, Forwood MR, Johnston CC, Burr DB (2000) Suppressed bone turnover by bisphosphonates increases microdamage accumulation and reduces some biomechanical properties in dog rib. J Bone Miner Res 15:613–620
42. Mashiba T, Mori S, Burr DB, Komatsubara S, Cao Y, Manabe T, Norimatsu H (2005) The effects of suppressed bone remodeling by bisphosphonates on microdamage accumulation and degree of mineralization in the cortical bone of dog rib. J Bone Miner Metab 23(Suppl):36–42
43. Hashimoto J, Yoshikawa H, Takaoka K, Shimizu N, Masuhara K, Tsuda T, Miyamoto S, Ono K (1989) Inhibitory effects of tumor necrosis factor alpha on fracture healing in rats. Bone 10:453–457
44. Reumann MK, Nair T, Strachna O, Boskey AL, Mayer-Kuckuk P (2010) Production of VEGF receptor 1 and 2 mRNA and protein during endochondral bone repair is differential and healing phase specific. J Appl Physiol 109:1930–1938
45. Everts V, de Vries TJ, Helfrich MH (2009) Osteoclast heterogeneity: lessons from osteopetrosis and inflammatory conditions. Biochim Biophys Acta 1792:757–765
46. Cecchini MG, Hofstetter W, Halasy J, Wetterwald A, Felix R (1997) Role of CSF-1 in bone and bone marrow development. Mol Reprod Dev 46:75–83
47. Wiktor-Jedrzejczak W, Urbanowska E, Aukerman SL, Pollard JW, Stanley ER, Ralph P, Ansari AA, Sell KW, Szperl M (1991) Correction by CSF-1 of defects in the osteopetrotic op/op mouse suggests local, developmental, and humoral requirements for this growth factor. Exp Hematol 19:1049–1054
48. Rawlinson SC, McKay IJ, Ghuman M, Wellmann C, Ryan P, Prajaneh S, Zaman G, Hughes FJ, Kingsmill VJ (2009) Adult rat bones maintain distinct regionalized expression of markers associated with their development. PLoS One 4:e8358
49. Varanasi SS, Olstad OK, Swan DC, Sanderson P, Gautvik VT, Reppe S, Francis RM, Gautvik KM, Datta HK (2010) Skeletal site-related variation in human trabecular bone transcriptome and signaling. PLoS One 5:e10692